

SPECTROSCOPIC DETECTION OF THE 3.934 MICRON LINE OF Si IX IN THE SOLAR CORONA

P. G. JUDGE AND S. TOMCZYK

High Altitude Observatory, National Center for Atmospheric Research,¹ P.O. Box 3000, Boulder CO 80307-3000; judge@ucar.edu

AND

W. C. LIVINGSTON, C. U. KELLER, AND M. J. PENN

National Solar Observatory,² P.O. Box 26732, Tucson, AZ 85726

Received 2002 May 24; accepted 2002 July 26; published 2002 August 12

ABSTRACT

We report the detection of the $2s^2 2p^2 \ ^3P_{1 \rightarrow 0}$ line of Si IX using the McMath-Pierce telescope on Kitt Peak. Observations were made of the solar disk and at various heights above the limb between 2002 May 13 and 17, under nonideal sky conditions, using the 13.5 m vertical spectrograph and an InSb single-diode detector. We report a new rest wavelength for the line and discuss its potential use as a diagnostic of coronal magnetic fields using ground-based telescopes. Our observations give $\lambda_{\text{rest}} = 3.93434 \pm 0.00007 \ \mu\text{m}$, consistent with earlier less accurate values, but it places the blue wing of the line under a strong telluric N₂O line. In the active regions observed, the line's intensity is comparable to or larger than predicted in earlier work for the quiet Sun.

Subject headings: Sun: corona — Sun: infrared

1. INTRODUCTION

Coronal physics has been boosted enormously over the last decade with the advent of data from the *Yohkoh*, *Solar and Heliospheric Observatory (SOHO)*, and *Transition Region and Coronal Explorer* spacecrafts. Yet critical questions remain open and will likely remain so until we can reliably measure coronal magnetic fields. While strong coronal fields ($B > 200$ G) located above active regions can be measured using radio techniques, the weaker fields characteristic of most of the corona require other methods. Judge et al. (2001) argued that the forbidden coronal emission lines show the greatest promise, through two effects: the Zeeman effect and scattering polarization. Recent work with the Evans 40 cm coronagraph (Lin, Penn, & Tomczyk 2000) proves that the high-precision measurements needed for the Zeeman effect can be done for the Fe XIII 1.0747 μm line. Similar measurements are an important goal of the Advanced Technology Solar Telescope (ATST). Design studies for the ATST show that coronal measurements will potentially be far easier in the thermal IR (3–5 μm) than at shorter wavelengths.

Judge (1998) identified a promising transition of Si IX near 3.9346 μm that is predicted to be strong ($12B_{-6}$ at 100" above the quiet Sun, where $1B_{-6} \equiv 1$ millionth of the disk intensity) and is favorably placed in wavelength (Judge et al. 2001). W. C. Livingston (1997, unpublished) derived an upper limit of $1B_{-6}$ using the McMath-Pierce telescope on 1997 December 9, a period close to solar minimum. Kuhn et al. (1999) reported a 2σ "probable discovery" of this line from an aircraft platform using a narrowband filter system during the 1998 February 26 total eclipse. These experiments failed to provide conclusive evidence that the line is strong enough to warrant serious consideration for coronal magnetometry. Here we report a definitive detection of the line in the active corona. We discuss its observed properties in relation to the proposed use of the line for ground-based coronal magnetometry.

2. OBSERVATIONS

Observations of the corona were attempted from 2002 May 12 to 17. Sky conditions were never "coronal": at best, a visible aureole could be seen, and at worst, high cirrus clouds were present. Each day, two or more bright active region loop systems were present above the solar limb in images from the EUV Imaging Telescope on board *SOHO*. In consultation with the weekly planner (P. Gallagher) for the Coronal Diagnostic Spectrometer (CDS) instrument on *SOHO*, a primary target was selected for the McMath-Pierce observations, although we observed several regions each day.

Our measurements were subject to important sources of unwanted signals: atmospheric scattering, emission, absorption, and even scattering from birds and other objects, which in principle can change on timescales of seconds, as well as scattered light and thermal emission from the telescope, spectrograph, and components in the cryogenic "Babo" Dewar used, which should vary much more slowly. Steps were taken to reduce the unwanted nonatmospheric signals. The telescope mirrors were cleaned on 2002 May 9 and 10, which significantly reduced the telescope-scattered light. Spectral scans were taken with a moderate cadence (10–20 s) using the rapid scan photometry system developed by J. Brault. Such chopping minimizes the effects of thermal emission arising from the telescope/spectrograph/detector system, so there should be no uncompensated thermal emission in our data. Similar systems have been widely used for photometry and are linear over many orders of magnitude (R. Joyce 2002, private communication).

Our instrumental setup was similar to that described by Livingston (1991). Light from the main McMath-Pierce telescope was focused onto a 0.5 mm wide, 10 mm long slit at the entrance to the main spectrograph. At the entrance slit the image scale is 2.5 mm⁻¹. We observed in third order for optimal throughput. At an exit port of the spectrograph, the light was directed into the Babo Dewar, where light passed through a cold 0.2 mm wide exit slit and a filter (OCLI 04048-4) centered near 4 μm with a passband of $\pm 0.1 \ \mu\text{m}$, required to reject unwanted light. A concave mirror in the Dewar focused the light onto a single InSb diode, whose current was proportional to the flux of incident radiation. Spectral scans spanning typically 0.007 or 0.014 μm were acquired through forward and

¹ The National Center for Atmospheric Research is sponsored by the National Science Foundation.

² The National Solar Observatory is operated by the Association of Universities for Research in Astronomy, Inc., under cooperative agreement with the National Science Foundation.

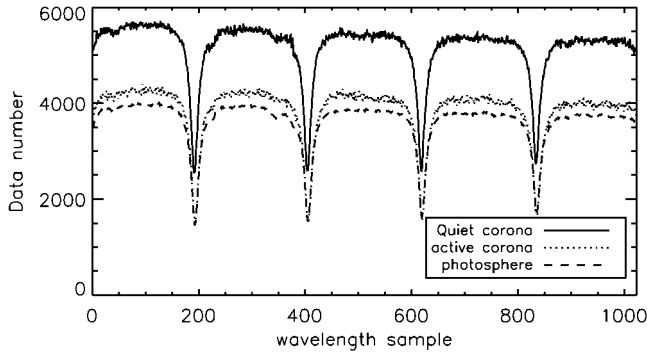


FIG. 1.—Typical raw spectral integrations, from 2002 May 14. The four deep absorption features are telluric N_2O separated by roughly $0.0015 \mu\text{m}$. Si IX coronal emission near $3.9343 \mu\text{m}$ is difficult to see in this figure, but it lies between wavelength samples 450 and 500 in the active coronal integration.

backward rotations of the grating. The data acquisition system performed two tasks: (1) Unwanted thermal radiation and non-zero offset in the detector amplifier were measured at the end of each scan and subtracted from the data, effectively removing variations and drift (“ $1/f$ noise”). These (dark) signals were measured during a short interval when a shutter under the entrance slit closed. (2) Thermal radiation from the shutter itself was determined and subtracted during initialization of each scan. Thus, all detector and spectrograph dark signals were removed by chopping at the scan cadence. The thermal background contributes high-frequency noise, but this proved negligible compared to telescope and sky noise. Each backward/forward pair of scans was averaged, and between 50 and 400 such pairs were summed and written to file. This average is henceforth referred to as one “integration,” of typically between 5 and 20 minutes duration.

Remaining sources of error arise only by variable atmospheric and solar properties, slowly varying instrumental properties, and additional uncertainties arising from neutral density (ND) filters and different amplifier gains used when observing the solar disk. These we try to correct a posteriori from the data themselves. A sky measurement made 30° from the Sun yielded count rates corresponding to $78B_{-6}$. This value, converted to the appropriate data number, was subtracted from each integration.

The spectral resolution of $\approx 0.7 \text{ \AA}$, set by the entrance slit width, exceeds by a factor of 7 the expected width of a Doppler-broadened coronal line near $4 \mu\text{m}$. This resolution was over-sampled in wavelength by an additional factor of 10, allowing us to use the highest wavenumbers in the Fourier transforms to estimate random components of the noise. Figure 1 shows some typical raw data. A (small) slope seen in the data results from a residual photometric error discussed below. The deep absorption features are telluric N_2O , and the shallow absorption features arise from telluric and solar lines. Characteristic patterns in such spectra were used to identify the observed wavelength region using the atlas of Livingston & Wallace (1991).

Intensity calibration was done via disk observations made through the ND filters with the gain on the Dewar’s amplifier set via a switch to $\times 1$. Coronal measurements were made with the switch set to $\times 10$. With the assumption that the diode’s response is linear, the ND filter transmissions were determined to be 0.098 and $0.092 \pm \approx 5\%$ using a fixed gain on the Dewar’s amplifier. Using the transmission of one of the ND filters, the Dewar $\times 10$ gain was found to be actually $10.6 \pm 10\%$. Disk observations were thus made with a sensitivity 1200 ± 150

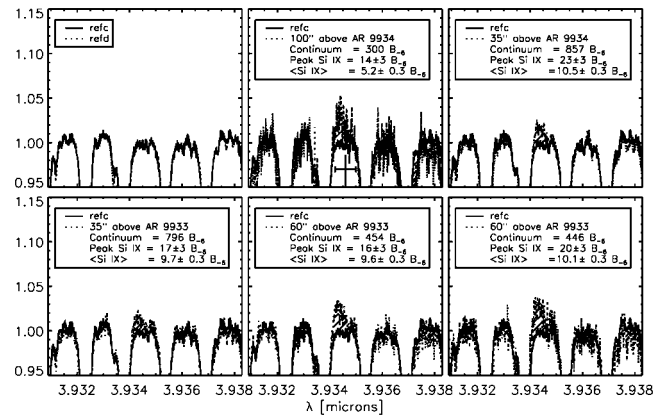


FIG. 2.—Detection of the $2s^2 2p^2 \ ^3P_{1-0}$ line of Si IX above active regions in the solar corona, observed on 2002 May 14. Upper left panel compares disk spectra and a spectrum obtained $35''$ above the northern coronal hole. Other panels compare the coronal hole spectrum with those above active regions. All are normalized so that the continuum is unity. Hatched areas highlight the differences between the coronal hole and active region spectra. The legends list continuum intensities and peak and net average intensities of the Si IX emission, all in units of B_{-6} , which is one millionth of the disk intensity. Error bar plotted in the upper middle panel shows the rest wavelength estimated by Oliva et al. (1994).

times smaller than those made of the corona. The quoted uncertainty is a lower limit because it does not include errors from (1) nonlinearities in the amplifier on the InSb diode, (2) secular variations of the gain with time, (3) contributions from variations of intensity across the disk, (4) the fact that the filters placed in series contribute thermal emission to and reflection of the beam, (5) secular variations in atmospheric conditions, and (6) the fact that the offset of $78B_{-6}$, of unknown origin, may or may not be applicable to disk data. Error source 1 should be negligible for the Babo system. It was not possible to disentangle sources 2 and 5, but their net effect appears to be on the order of 5%, judging from variations seen in the disk data sets obtained on 2002 May 16. We took data within the central 90% of the solar disk, over which center-to-limb intensity variations are $\leq 10\%$ at $4 \mu\text{m}$ (Allen 1973). By tilting the ND filters slightly, the measured transmission changed by $\approx 1\%$, suggesting that additional uncertainties introduced by the filters are of this magnitude. Thermal emission from the ND filters introduces less than a Planck function of intensity into the beam at 300 K and competes with 0.01 of the disk intensity at the entrance slit. The solar light exceeds thermal emission from the filters by at least 900. Errors arising from source 6 are on the order of 10%. Propagation of the known uncertainties yields a net uncertainty of $\pm 20\%$, which is a lower limit because of the unknown affects of error sources 2 and 5.

Coronal integrations were made at various heights between $12.5''$ and $100''$ above the solar limb, with the projected slit oriented tangentially to it. Because of the strong background, we integrated over active and quiet corona and subtracted the latter data to reveal excess emission.

3. RESULTS

Coronal Si IX was unambiguously detected on 2002 May 14 over the two active regions with bright loops over the west limb, AR 9934 and AR 9933 (Fig. 2). It was not detected on 2002 May 13, 15, or 16, but was seen (less clearly) on May 17. The line was most easily detected on the day with the darkest sky. The continuum brightness near $3.9 \mu\text{m}$ measured

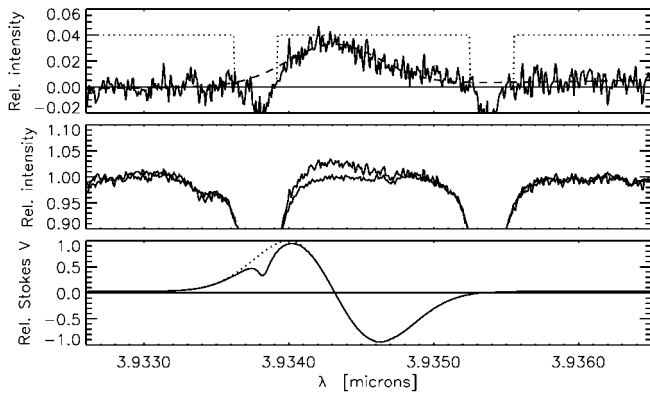


Fig. 3.—Single-component Gaussian fit to the line profile obtained by summing data obtained $60''$ above AR 9933 and subtracting the coronal reference spectrum REFC according to eq. (1). *Upper panel:* Data and fit, with relative weights shown with dropouts where telluric absorption has spuriously affected the derived spectrum. *Middle panel:* Summed data and REFC. *Lower panel:* Wavelength derivative of the fit and the derivative but multiplied by an approximate atmospheric transmission function, taken directly from the data.

above the limb, of atmospheric and instrumental origin, varied from day to day. For example, $60''$ above the limb it varied between $500B_{-6}$ and $1100B_{-6}$. During each day the brightness typically varied by $\pm 20\%$ at a given height above the limb, with occasional excursions of a factor of 2 during cloudy conditions. No obvious variations on shorter timescales were evident on the data acquisition display. Thus, scattered atmospheric light contributed a significant fraction of the off-limb measured brightnesses.

To improve signal-to-noise ratios, we coregistered and summed integrations acquired with the same pointing. Each integration was also “detrended,” to correct for the linear slope continuum slope seen in Figure 1, by dividing each integration by a function of the form $a + b\lambda$. This ad hoc correction, discussed further below, is needed because the solar continuum is essentially flat (Farmer & Norton 1989). We defined two “reference” data sets, “REFD” and “REFC,” corresponding to spectra obtained on the disk and in the dim corona away from active regions. Wavelength coregistration, calibration, and intensity calibrations were done using REFD. The REFC data sets were compared and subtracted from integrations of the corona over active regions to search for coronal emission. Figure 2 shows integrations from 2002 May 14 when the line was obviously detected in five separate integrations over two active regions. Noise levels estimated from high-wavenumber parts of the Fourier transforms of the spectra yield rms errors of $0.3B_{-6}$, showing that each of these detections is formally at a significance of between 16 and 30σ , not counting systematic errors. We know of no source of systematic error that can qual-

itatively produce the observed Gaussian line profiles. Thus, *this is the first definitive detection of the Si IX line from the solar corona*. The lower signal-to-noise ratios for the May 13 and 15–17 data sets are compatible with this result, with a 7σ detection recorded on May 17 above a northeast active region.

A linear wavelength calibration was performed using the telluric lines of N_2O , whose wavelengths are known to three parts in $\times 10^9$ (National Institute of Standards and Technology spectroscopic database), from which we determined a new rest wavelength from the mean of several Gaussian fits to the net profiles (data minus REFC) obtained on May 14. Figure 3 shows a fit to the summed data obtained $60''$ above AR 9933. The fit was to a linear background plus Gaussian profile using a standard least-squares routine. Standard weights for χ^2 minimization were determined from the random component of the noise except at wavelengths where obvious residual telluric effects were present, when the weights were set to zero (see Fig. 3); χ^2 varied from 2.5 to 9.5 for the data shown in Figure 2. Thus, either systematic sources of error are important and/or the random components of the noise have been underestimated. Table 1 lists the best-fit parameters for three out of the five coronal integrations shown in Figure 2 for which fits could be obtained. Also listed is a fit to the following function, which attempts to take care of variations in the telluric features and scattered light:

$$y = \text{data} - (a + b \times \text{REFC}), \quad (1)$$

for the summed data obtained $60''$ above AR 9933. For this data set, $a = 0.0296$ and $b = 0.9641$ were determined by minimizing the sum of the absolute values of y in spectral regions away from the coronal emission line. The uncertainties listed in the table are formal errors only. The rms variation of λ_{fit} for the coronal integrations listed in Table 1 is $0.00007\ \mu\text{m}$, 10 times larger than the formal uncertainties. AR 9934 is systematically redshifted by $\approx 10\sigma$ relative to AR 9933 by $10\ \text{km s}^{-1}$ ($0.00015\ \mu\text{m}$). Coronal forbidden lines routinely show several kilometers per second Doppler shifts in different regions (e.g., Tsubaki 1975), but we warn against overinterpretation of these results given the difficulties in dealing with telluric absorption. Adopting $0.00007\ \mu\text{m}$ rms variation as our wavelength uncertainty, we find

$$\lambda_{\text{rest}} = 3.93434 \pm 0.00007\ \mu\text{m},$$

where our revised estimate of the rest wavelength $\lambda_{\text{rest}} = \lambda_{\text{fit}}(1 - v_r/c)$ and v_r is the solar rotation rate close to the west limb (a value of $1.95\ \text{km s}^{-1}$ appropriate to $\pm 20^\circ$ latitudes of the observed active regions was used). Additional corrections (Earth-Sun motion and gravitational redshifts) are negligibly

TABLE 1
GAUSSIAN FITS FOR DATA OBTAINED ON 2002 MAY 14

Target	χ^2	I_{peak}^a (B_{-6})	$\int I_\lambda d\lambda^b$ ($\text{ergs cm}^{-2} \text{s}^{-1} \text{sr}^{-1}$)	λ_{fit} (μm)	FWHM (km s^{-1})
$100''$ above AR 9934	9.85	12.4	0.9	3.934450 ± 0.000005	38.3 ± 1.0
$35''$ above AR 9934	4.54	19.4	1.4	3.934396 ± 0.000005	39.1 ± 1.0
$60''$ above AR 9933	2.66	13.7	1.6	3.934299 ± 0.000009	62.0 ± 1.8
$60''$ above AR 9933 ^c	2.64	14.1	1.5	3.934312 ± 0.000007	56.9 ± 1.4

^a All intensities have uncertainties of at least $\pm 20\%$ (see text).

^b For comparison, Judge 1998 computed a value of $0.68\ \text{ergs cm}^{-2} \text{s}^{-1} \text{sr}^{-1}$ over a typical quiet region of the corona (see text); with an FWHM of $40\ \text{km s}^{-1}$, this yields $I_{\text{peak}} \approx 12B_{-6}$.

^c These results were evaluated using eq. (1) as discussed in the text.

small. The telluric absorber in principle limits the accuracy with which we can determine λ_{rest} . However, the above uncertainty seems reasonable given that the fitted line widths are compatible with predictions, suggesting that the Gaussian fits have captured enough of the blue side of the emission line to render the fitted central wavelength and its uncertainty believable. This measurement supersedes and agrees with the best previous estimate of $3.9346 \pm 0.0004 \mu\text{m}$, derived from spectra of active galactic nuclei (Oliva et al. 1994).

In summary, the measured wavelengths, peak intensities, and widths listed in Table 1 are compatible with earlier predictions for the Si IX coronal line (e.g., Oliva et al. 1994; Judge 1998). The longitudinal Zeeman splitting is a negligible contributor to the line width, being on the order of $10^{-5} B \text{ (G)} / 100 \mu\text{m}$ compared with $\text{FWHM} = 9.5 \times 10^{-4} \mu\text{m}$.

4. DISCUSSION

Our data show that the $2s^2 2p^2 \ ^3P_{1-0}$ line of Si IX is present in active regions at intensity levels similar to or larger than those predicted for the quiet Sun by Judge (1998). The line might have been expected to be stronger than observed. This difference may be due to variations in the silicon abundance in the corona. Judge used a coronal abundance of 8.00, compared with a photospheric value of 7.52 (e.g., Allen 1973). Also, a small relative enhancement of the line in active over quiet regions may result from the small radiative transition probability of the line (Brage et al. 2000) compared with the larger collisional deexcitation probabilities that are present in active region plasma.

Several sources of systematic error are present in our data. One source is revealed through discontinuities in plots of equivalent widths of telluric features with air mass. Our 5–20 minute long integrations are susceptible to low-frequency noise outside of the Dewar, which introduces occasional discontinuities in the continuum. On 2002 May 14, such discontinuous changes coincide with changes in the pointing from high in the corona to lower levels. The changes also correlate with the poorly understood slope in the data and with the number of counts accumulated during each integration. These correlations are consistent with an external source of low-frequency noise (such

as clouds) in the data, of proportionately greater importance in longer integrations containing intrinsically weaker signals. Figure 2 shows data corrected for this slope, but a similar uncorrected plot clearly shows the presence of the emission line. Thus, our detection does not hinge upon this noise source. We cannot think of any source of error that might offer a credible explanation for the Gaussian-like emission profile behavior exhibited by the data. However, uncompensated systematic errors are worrisome and can affect the measured line profile parameters, so we performed additional tests. By varying the treatment of the $78B_{-6}$ background (sloped vs. constant vs. zero) and the telluric absorption (according to whether eq. [1] was applied), neither the quoted significance of the detection nor the quoted rest wavelength or line width are significantly affected.

We conclude that the $2s^2 2p^2 \ ^3P_{1-0}$ line of Si IX remains a strong candidate for coronal magnetometry studies using new facilities, such as ATST. One potential problem arises: our revised wavelength places the blue wing of the line under a strong N_2O telluric absorber. The lower panel of Figure 3 indicates the telluric influence on a representative Stokes V profile. Calculations show that N_2O has significant absorption above even 8 km altitude (D. Edwards & E. Francis 1997, private communication), so ground-based Stokes polarimetry will have to take this into account. Nevertheless, with a good coronagraph and clearer skies, the signal-to-noise ratio will improve enormously, enabling spectropolarimetric measurements of the coronal magnetic field with this line. In passing we note that a recent revision of the rest wavelength for the $2s^2 2p^2 \ ^3P_{3/2 \rightarrow 1/2}^o$ line of Mg VIII ($3.027648 \pm 0.000020 \mu\text{m}$; Casassus, Roche, & Barlow 2000) fortuitously places the line further from a water vapor absorber (see Fig. 14 of Judge et al. 2001). This line is also potentially important for ground-based coronal magnetometry. We intend to measure this line with the McMath-Pierce telescope, following an early 3σ detection by Münch, Neugebauer, & McCammon (1967). Finally, the CDS team acquired data in EUV lines of Si IX in the active regions observed with the McMath-Pierce telescope. These data will be analyzed in a future publication.

We thank Peter Gallagher and Andrzej Fludra for help in identifying targets from *SOHO* data and Tim Brown and Jeff Kuhn for helpful comments on the manuscript.

REFERENCES

- Allen, C. W. 1973, *Astrophysical Quantities* (London: Athlone)
- Brage, T., Judge, P. G., Joensson, P., & Edwards, D. P. 2000, *ApJ*, 540, 1114
- Casassus, S., Roche, P. F., & Barlow, M. J. 2000, *MNRAS*, 314, 657
- Farmer, C. B., & Norton, R. H. 1989, *A High-Resolution Atlas of the Infrared Spectrum of the Sun and the Earth Atmosphere from Space* (NASA RP-1224 ; Washington, DC: NASA)
- Judge, P. G. 1998, *ApJ*, 500, 1009
- Judge, P. G., Casini, R., Tomczyk, S., Edwards, D. P., & Francis, E. 2001, *Coronal Magnetometry: A Feasibility Study* (NCAR Tech. Note 446+STR)
- Kuhn, J., et al. 1999, *ApJ*, 521, 478
- Lin, H., Penn, M. J., & Tomczyk, S. 2000, *ApJ*, 541, L83
- Livingston, W. C. 1991, in *Proc. 11th NSO/Sacramento Peak Summer Workshop, Solar Polarimetry*, ed. L. J. November (Sunspot: NSO), 356
- Livingston, W. C., & Wallace, L. 1991, *An Atlas of the Solar Spectrum in the Infrared from 1850 to 9000 cm^{-1} (1.1 to 5.4 μm)* (NSO Tech. Rep. 91-001; Tucson: NSO)
- Münch, G., Neugebauer, G., & McCammon, D. 1967, *ApJ*, 149, 681
- Oliva, E., Salvati, M., Moorwood, A. F. M., & Marconi, A. 1994, *A&A*, 288, 457
- Tsubaki, T. 1975, *Sol. Phys.*, 43, 147